Inertia-gravity waves in Antarctica: Using ray tracing to study measurements at McMurdo/Scott Base (77.83° S, 166.67° E)

R. Michael Jones[a], Xinzhao Chu[a], Jackson Jandreau[a], & others?[a]

[a]*Cooperative Institute for Research in Environmental Sciences, University of Colorado, Boulder, Colorado 80309-0216, U.S.A.*

Abstract

The NOAA/CIRES ray-tracing program is used to learn more about the characteristics of the gravity waves that were inferred from temperature profiles measured with the ground-based LIDAR at McMurdo/Scott Base in Antarctica on 29 June 2011 [Chen et al. 2013, Journal of Geophysical Research: Atmospheres 118 (7), 2794-2808]. The ray-path calculations show that the gravity waves deviate significantly from a great circle path because of wind. The source of the 7.7-hour gravity wave is estimated to be at a height between 50 and 75 km in the atmosphere at a longitude of about 100° west off the coast of Antarctica, but the source could be lower and further West if it is farther away. Using reverse ray tracing improves the efficiency of estimating the source location of the gravity waves. The usual formula for the acoustic-gravity wave dispersion relation (that depends on only the vertical component of the Earth's angular velocity in the Coriolis force) gives the correct low-frequency cut off, but including all components of the Earth's angular velocity gives more accurate propagation calculations in some cases.

Keywords: gravity waves, Antarctica, ray tracing

1. Introduction

Atmospheric gravity waves perturb the temperature and wind as they propagate. Measuring temperature profiles using LIDAR shows that gravity waves with periods ranging from 3 to 10 hours are typical in Antarctica (Chu et al., 2011; Chen et al., 2013, 2016; Zhao et al., 2017; Chu et al., 2018). Two gravity waves were measured on 29 June 2011 in the height range from 81 km to 107 km above the research station at McMurdo in Antarctica, one gravity wave with a 5.0-hour period and one gravity wave with a 7.7-hour period (Chen et al., 2013).

The 7.7-hour gravity wave had a vertical wavelength of about 22 km, a horizontal wavelength of about 2200 km, a horizontal group speed of about 48 m/s, vertical group speed of about 0.5 m/s upward, propagating in an azimuth direction of about 11° clockwise from north (Chen et al., 2013). The phase propagation was downward. Because the group velocity was nearly horizontal, the source was estimated to be in the stratosphere just off the coast of Antarctica near the prime meridian.

To illustrate how ray tracing can help give more information about measured gravity waves, we use the CIRES/NOAA ray-tracing program to investigate the 7.7-hour gravity wave.

We start by using the temperature and wind information from McMurdo as being representative of the temperature and wind in the region to make calculations of gravity waves that we can compare with the observations. As will be seen, the assumption of uniform temperature and wind profiles gives results that are in reasonable agreement with the measurements, but some disagreements show that the assumption of a uniform temperature and wind velocity cannot be exactly correct. In addition, the presence of significant wind causes the gravity waves to deviate significantly from a great-circle path, showing that the source of the gravity waves is significantly to the west of the prime meridian.

The CIRES/NOAA acoustic-gravity wave ray tracing computer program used for these calculations is a general three-dimensional ray tracing program for calculating acoustic-gravity waves in the atmosphere (described in Bedard and Jones, 2013; Jones and Bedard, 2015, 2018) based on an earlier program HARPA for calculating the propagation of acoustic waves (Jones et al., 1986a,b; Georges et al., 1990). The ray tracing program calculates ray paths by integrating Hamilton's equations in Earth-centered spherical polar coordinates (Jones et al., 1986a, pp. 89-91).

Jones (1996) reviews the practical aspects of ray tracing, the WKB approximation, and the limits of geometrical optics to calculate wave propagation in the atmosphere. Although the WKB approximation was given its present name after 1926 (Wentzel, 1926; Kramers, 1926; Brillouin, 1926), the method was discovered earlier (Liouville, 1836, 1837a,b; Rayleigh (John William Strutt), 1912; Jeffreys, 1923).

Section 2 presents the atmospheric temperature and wind profiles used in the calculations. Section 3 shows the appropriate ray-path calculations and profile calculations. Section 4 uses reverse ray tracing to estimate the source location of the gravity waves. Section 5 includes more height detail in the wind profile. Section 6 considers the spatial variation in the temperature and wind profiles. Section 7 presents the conclusions.

To correctly interpret gravity wave measurements at such low frequencies with ray tracing calculations requires an accurate representation of the effect of Coriolis force on the propagation. Although the usual dispersion relation (Eckart, 1960, eq. (51-2), p. 125) (Gossard and Hooke, 1975, eq. (23-7), p. 112)

that includes the effect of only the vertical component of the Earth's angular velocity on the Coriolis force[1] gives the correct low-frequency cut off for inertial gravity waves, it neglects possibly significant effects from the horizontal components of the Earth's angular velocity. The appendices show situations where neglecting the horizontal components of the Coriolis force gives ray paths that differ from those that include all components of the Coriolis force.

Appendix A gives the usual barotropic dispersion relation that includes only the vertical component of the Earth's angular velocity. Appendix B gives the barotropic dispersion relation that includes all components of the Earth's angular velocity. Appendix C shows a comparison of the ray paths and vertical-wavelength profiles resulting from the two versions of the dispersion relation. Appendix D points out there are situations where all components on the Earth's angular velocity should be included in the Coriolis force terms in the dispersion relation. Appendix E gives an approximate dispersion relation that neglects rate-of-strain and baroclinicity, but still includes the effects of all components of the Earth's angular velocity on the Coriolis force.

2. The atmospheric model

As a first approximation to calculate ray paths, we use a temperature profile appropriate to McMurdo, Antarctica for 29 June 2011, 20 UT, as shown in figure 1. The corresponding Brunt-Väisälä frequency profile is shown in figure 2.

Figure 3 shows the eastward component of the wind at McMurdo Station for 29 June 2011 measured (circles) and as used in the ray-path calculations (solid line). As pointed out by Chen et al. (2013), the measured profile includes gravity-wave associated variations (Chen et al., 2013, figure 2), which would not be appropriate to use in making the ray-path calculations. The north-south components of the wind velocity profile were much smaller than the east-west components, and we neglect them for the calculations here. As a first approximation, we use the same wind profile for the entire propagation region.

3. Ray-path and profile calculations

Many gravity waves (including the 7.7-hour gravity wave studied here) are in the category of asymptotic gravity waves, that have a wave-normal direction that is at an angle of $\cos^{-1} \omega_i/N$ from the horizontal, where ω_i is the intrinsic frequency (the frequency in a frame moving with the wind) and N is the Brunt-Väisälä frequency. The wave frequency of a gravity wave with a period of 7.7 hours is so low that wave-normal directions would be within a degree or so of vertical, and the corresponding ray directions would be nearly horizontal. In addition, as is well known, the vertical component of the wave-normal direction is in the opposite direction from the vertical component of the ray direction. Because Chen et al.

[1] sometimes referred to as the "Shallow atmosphere" approximation (Phillips, 1966; Hickey and Cole, 1987)

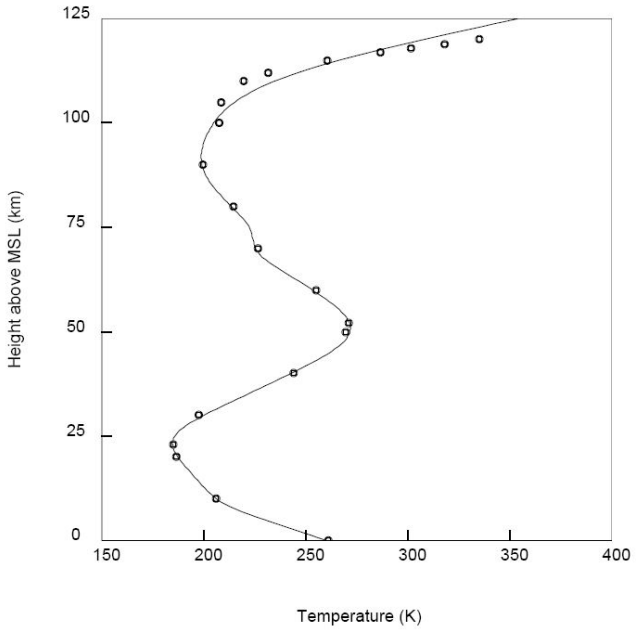

Figure 1: Temperature profile used in the ray path calculations. The circles are from the MSISE-00 model for McMurdo (77.83° S, 166.67° E) for 29 June 2011, 20 UT (NRLMSISE-00, Community Coordinated Modeling Center, 2016). The solid line is our fit to the profile that we used for the ray-path and profile calculations.

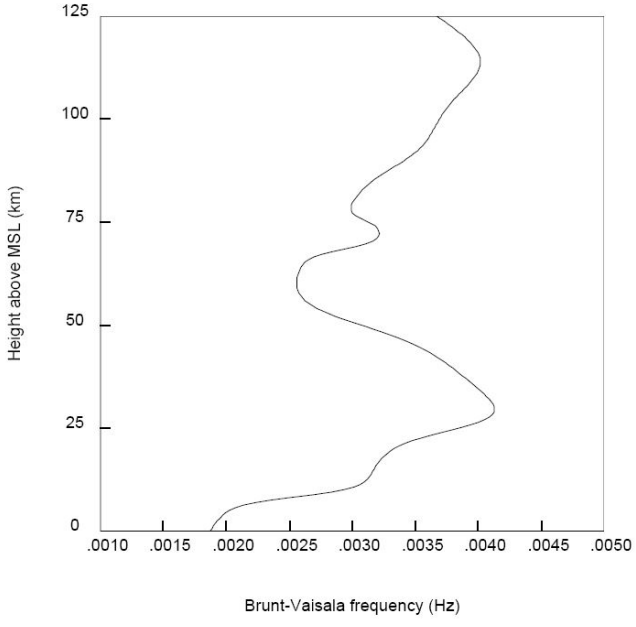

Figure 2: Brunt-Väisälä frequency profile for McMurdo (77.83° S, 166.67° E) for 29 June 2011, 20 UT corresponding to the temperature profile in figure 1.

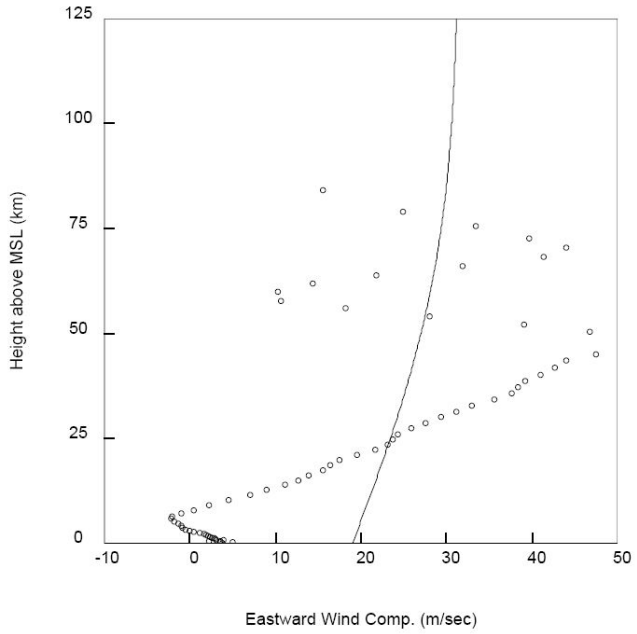

Figure 3: Eastward wind profile used for the ray-path and profile calculations (solid line). Measured wind profile for 29 June 2011 from MERRA-2 (circles) that includes the gravity-wave associated variability. The wind is blowing toward the East.

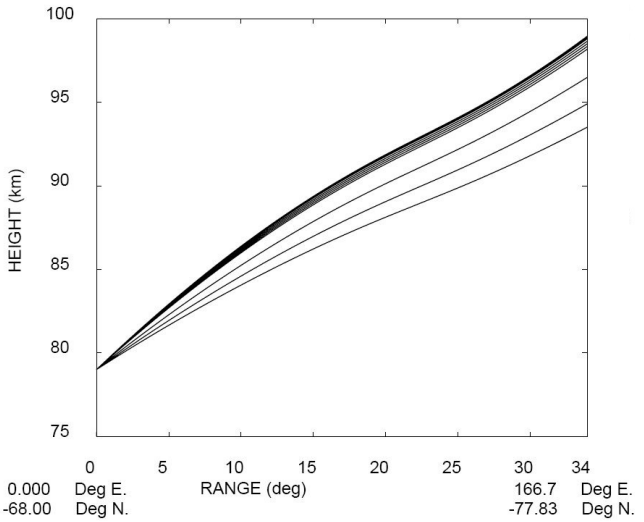

Figure 4: Projection of the ray paths on a vertical plane through the source and McMurdo Station for gravity waves with a period of 7.7 hours for various elevation angles of transmission. Notice that the vertical scale has been stretched, since the horizontal range is about 3773 km. These ray paths are nearly horizontal. The elevation angles of transmission (from bottom to top) are −89.0°, −89.1°,−89.2°, −89.3°, −89.31°, −89.32°, −89.33°, −89.34°, −89.341°, −89.342°, −89.343°, −89.344°, −89.345°, −89.346°, −89.347°, −89.348°, −89.349°, −89.35°, and −89.351°. The ray transmitted at an elevation angle of −89.349° came the closest to passing directly over McMurdo station. The wave-normal direction of that ray as it passed over McMurdo is −89.525° from horizontal and the vertical wavelength at that height of 98.935 km was 48.9 km. A ray transmitted at −89.352° was evanescent at the source. As is well known, the vertical component of the wave-normal direction is opposite to the vertical component of the ray direction for gravity waves. At such a low frequency, the wave-normal direction is nearly vertical and the ray direction is nearly horizontal.

(2013) observed the wave fronts of the 7.7 hour gravity wave to be moving downward, we calculate here ray paths for gravity waves in which the wave-normal elevation angle is about −89° (that is, down) with ray directions nearly horizontal, but moving slightly up.

Chen et al. (2013) estimated that these 7.7-hour gravity waves might have their source just off the coast of Antarctica near the prime meridian. Therefore, we decided to launch a series of rays from a longitude of zero and a latitude of 68° south. Because ray directions would be roughly horizontal, to get gravity waves that would pass over McMurdo within the height range of 80 to 100 km, required launching the gravity waves at some height in the atmosphere, and we eventually used a launch height of 79 km.

After some trial and error in launch directions (in both azimuth and elevation), we found some ray paths that went over McMurdo Station. These gravity waves were launched with an azimuth angle of 167.4° clockwise from north and elevation angles of −89° and steeper. These rays are shown in figures 4 and 5. The vertical wavelength of these gravity waves as they pass over McMurdo station is about 50 km.

For the steepest wave launched at a wave-normal direction of −89.351°, the wave-normal direction is 25.554° clockwise from north and −89.527° from horizontal at a height of 98.9615 km as the wave passed slightly to the south of McMurdo station.

The wave launched at a wave-normal direction of −89.349° passed directly over McMurdo station, where the wave-normal direction is 24.939° clockwise from north and −89.525° from horizontal at a height of 98.935 km.

The total travel time for these waves is about 8.6 hours. That gives an average horizontal speed of about 437 km/h or 121 m/s for the 3773 km total path. The average vertical speed would be about 0.6 m/s for the vertical climb from 79 to 99 km. The instantaneous velocity as the wave passes over McMurdo station would be slightly higher because of the curved ray path. The vertical component of the group velocity agrees reasonably well with that given by (Chen et al., 2013) of 0.5 m/s, but the horizontal component of the group velocity of 48 m/s given by (Chen et al., 2013) is much slower than the value given by the ray-path calculations.

The horizontal wavenumber of the gravity waves in figures 4 and 5 as they pass over McMurdo is about 10^{-3} km^{-1}. This corresponds to a horizontal wavelength of about 6000 km. The disagreement between calculations and measurements in group speeds is related to the disagreement in wavelengths, which is discussed later.

To be thorough, we should launch rays from different heights so that we can have rays passing over McMurdo at various heights from about 80 km up to 110 km. Instead, we calculate a vertical wavelength profile for gravity waves that match the gravity waves in figures 4 and 5 and that have a constant horizontal wavenumber. That profile is shown in figure 6. Notice that the wavelength of about 49 km at a height of 99 km agrees with that given by the ray-path calculations.

To match with the gravity-wave measurements of Chen et al. (2013) showing a vertical wavelength of about 20 km would re-

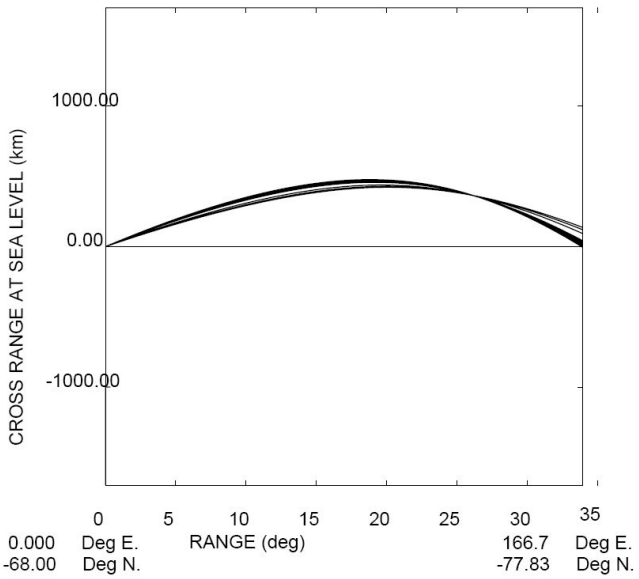

Figure 5: Projection of the ray paths from figure 4 on the ground. The great circle through the source and McMurdo Station is shown. The longitude and latitude of the two ends of the great-circle path are shown. The wave-normal direction of the wave that was transmitted at an elevation angle of −89.349° is 24.939° clockwise from north as it passes above McMurdo Station. Moving the source location farther west would give agreement with the azimuth angle of 11° clockwise of north given by Chen et al. (2013).

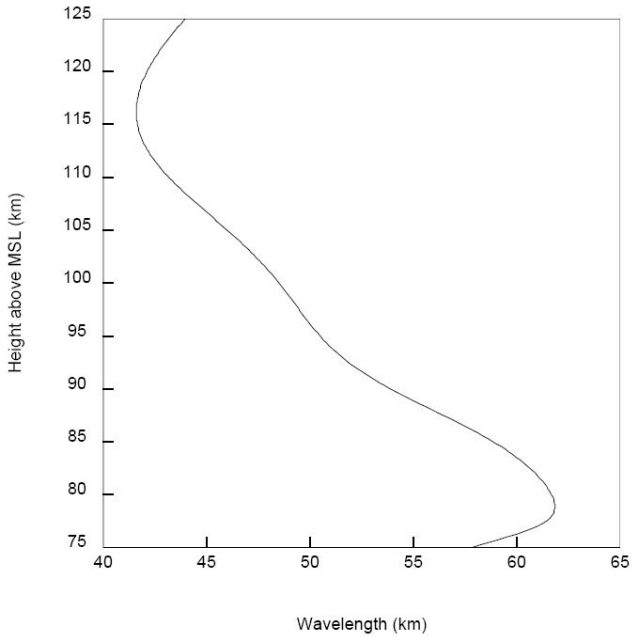

Figure 6: Wavelength profile above McMurdo Station for a wave-normal direction of −89.525° from horizontal and 24.939° clockwise from north at a height of 98.935 km. Since the wave-normal direction is nearly vertical, the wavelength and the vertical component of wavelength (actually 2π divided by the vertical component of the wavenumber) are nearly equal. The vertical wavelength at the height of 98.935 km is about 49 km, in agreement with the ray-path calculation as given in figure 4. The corresponding horizontal wavelength is about 5900 km, which is calculated from $(180/\pi) \times 49/(90 - 89.525)$.

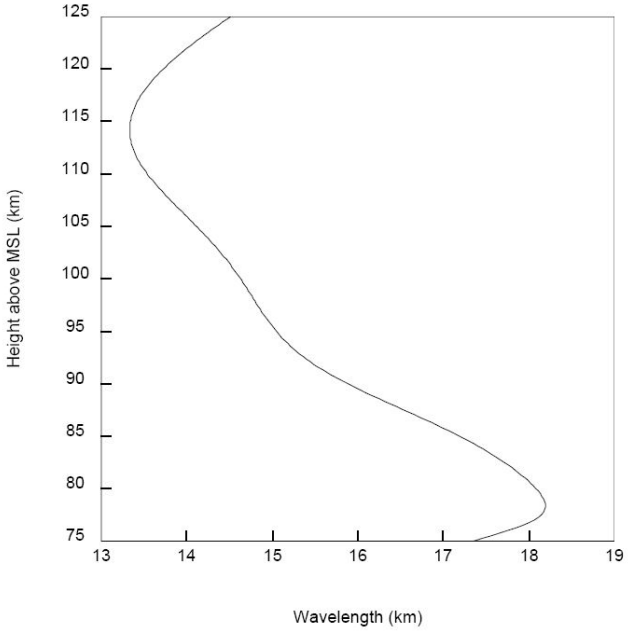

Figure 7: Wavelength profile above McMurdo Station for a wave-normal direction of 11° clockwise from north and −89.61° from vertical at a height of 98.935 km. The vertical wavelength at that height is about 14.75 km. The corresponding horizontal wavelength is about 2170 km.

quire slightly steeper ray paths than given in figures 4 and 5. However, in trying to launch steeper ray paths, we found that such waves would be evanescent at the source. Thus, the atmospheric conditions in Antarctica on 29 June 2011 must have been somewhat different from the horizontally uniform atmospheric models we used in our ray-path calculations.

Rather than try to estimate the atmospheric conditions between the source and McMurdo to perform raypath calculations, we instead calculate a vertical wavelength profile for McMurdo using a steeper elevation angle and that has an azimuth angle of 11° clockwise from north at a height of 98.935 km. This is shown in figure 7. As can be seen, the vertical wavelength varies between about 14 and 18 km, slightly smaller than the measurements at McMurdo on 29 June 2011, and the calculated horizontal wavelength is in reasonable agreement with the gravity-wave measurements on 29 June 2011.

The above ray-path calculations were made neglecting the horizontal components of the Earth's angular velocity in the Coriolis force. We also made ray-path calculations including all components of the Earth's angular velocity in the Coriolis force. The differences were very small for those cases, except that the ray that was launched at an elevation angle of −89.351° was evanescent at the source when all components of the Earth's angular velocity were included in the Coriolis force. However, the appendices show some situations where there are significant differences caused by neglecting the horizontal components of the Earth's angular velocity in the Coriolis forces.

Because the wind causes the gravity waves to deviate significantly from a great-circle path, the ray paths in figures 4 and 5 propagate in a different azimuth direction as they pass over McMurdo Station than was observed by Chen et al. (2013). To find

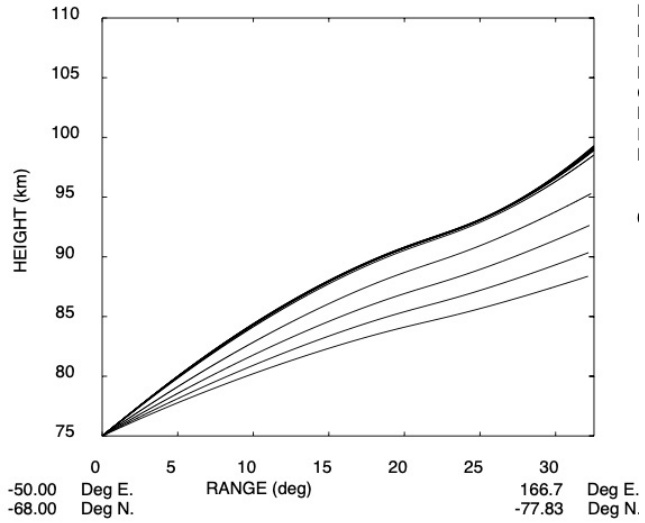

Figure 8: Projection of the ray paths on a vertical plane through the source and McMurdo Station for gravity waves with a period of 7.7 hours for various elevation angles of transmission. Notice that the vertical scale has been stretched, since the horizontal range is about 3617.5 km. These ray paths are nearly horizontal. The elevation angles of transmission (from bottom to top) are −89.0°, −89.1°,−89.2°, −89.3°, −89.4°, −89.41°, −89.411°, −89.412°, −89.413°, −89.414°, −89.415°, −89.416°, −89.417°, −89.418°, and −89.419°. The ray transmitted at an elevation angle of −89.416° came the closest to passing directly over McMurdo station. The wave-normal direction of that ray as it passed over McMurdo is −89.533° from horizontal and the vertical wavelength at that height of 99.2 km was 45 km. A ray transmitted at −89.420° was evanescent at the source. As is well known, the vertical component of the wave-normal direction is opposite to the vertical component of the ray direction for gravity waves. At such a low frequency, the wave-normal direction is nearly vertical and the ray direction is nearly horizontal.

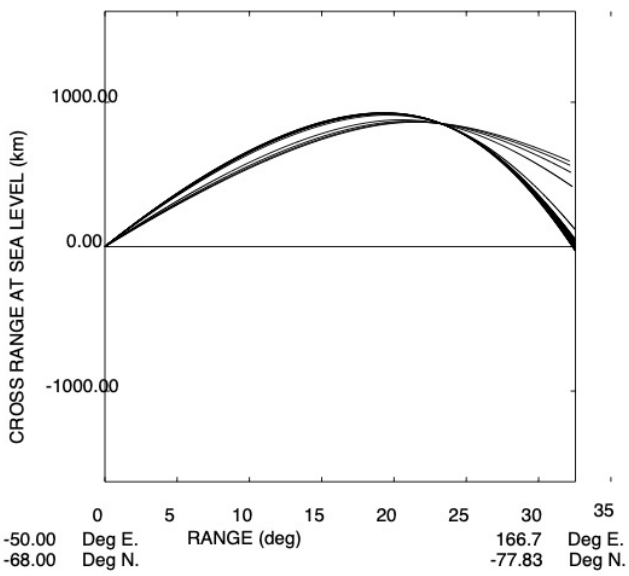

Figure 9: Projection of the ray paths from figure 8 on the ground. The great circle through the source and McMurdo Station is shown. The longitude and latitude of the two ends of the great-circle path are shown. The wave-normal direction of the wave that was transmitted at an elevation angle of −89.416° is 11.4° clockwise from north as it passes above McMurdo Station. This is reasonable agreement with the azimuth angle of 11° clockwise of north given by Chen et al. (2013).

gravity waves that propagate in the correct azimuth direction as they pass over McMurdo Station, we moved the source location west of the prime meridian. This resulted in the ray paths shown in figures 8 and 9. As with figures 4 and 5, the vertical wavelength of the gravity waves in figures 8 and 9 is significantly larger than was measured by Chen et al. (2013). To get gravity waves with the correct vertical wavelength as they pass over McMurdo Station would require steeper wave-normal directions, but these would be evanescent at the source, showing that the assumption of a horizontally uniform temperature and wind profile is not exactly correct.

The ray paths in figures 8 and 9 that passed over McMurdo were almost 100 km above the ground. To get gravity waves that pass over McMurdo at some of the lower heights where gravity waves were observed requires lowering the source height of the gravity waves. Figures (10) and (11) show ray paths for a source height of 60 km. The gravity waves that passed over McMurdo in those figures were about 87 km as they passed over McMurdo. To get gravity waves passing over McMurdo at a height of 80 km would require a lower source height, possibly about 50 km. If the source were even farther away, the height of the source would be even lower.

The ray path calculations shown neglect the horizontal components of the Earth's angular velocity in the Coriolis force. We also calculated the same ray paths including all components of the Earth's angular velocity. There were some slight differences. For example, the ray transmitted at an angle of −89.29° was evanescent at the source when including all components of the Earth's angular velocity. In addition, when including all components of the Earth's angular velocity, the ray transmitted at an elevation angle of -89.287 was the one that went over McMurdo at a height of 87.14 km at an angle of −89.47° from the horizontal and with an azimuth angle of 11.4° clockwise of North. The vertical wavelength was 137 km.

4. Reverse ray tracing

A more efficient way to search for the source of the gravity waves observed at McMurdo is to use reverse ray tracing. That is, we start a gravity wave at McMurdo and send it back where it came from by sending it back toward the direction it was seen coming from. To correctly do reverse ray tracing requires that the wind direction is reversed everywhere. We have done that, and the result is shown in figure 12. As can be seen, the effect of the wind on the ray paths is significant.

5. A new wind model

In the above analysis, we have treated the measured wind profile in figure 3 as though the roughly periodic variations of the wind with height was associated with the gravity wave. Another possibility is that the measured wind profile is the true background wind, and should be used in making ray-path calculations. To that end, we now use the wind model shown in figures 13 and 14.

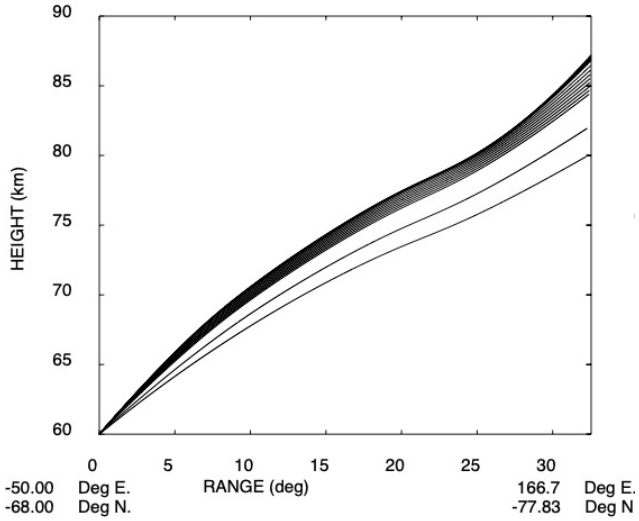

Figure 10: Projection of the ray paths on a vertical plane through the source and McMurdo Station for gravity waves with a period of 7.7 hours for various elevation angles of transmission. Notice that the vertical scale has been stretched, since the horizontal range is about 3617.5 km. These ray paths are nearly horizontal. The elevation angles of transmission (from bottom to top) are −89.0°, −89.1°, −89.2°, −89.21°, −89.22°, −89.23°, −89.24°, −89.25°, −89.26°, −89.27°, −89.28°, −89.281°, −89.282°, −89.283°, −89.284°, −89.285°, −89.286°, −89.287°, −89.288°, and −89.29°. The ray transmitted at an elevation angle of −89.288° came the closest to passing directly over McMurdo station. The wave-normal direction of that ray as it passed over McMurdo is −89.469° from horizontal and the vertical wavelength at that height of 87.1 km was 116 km. A ray transmitted at −89.3° was evanescent at the source. As is well known, the vertical component of the wave-normal direction is opposite to the vertical component of the ray direction for gravity waves. At such a low frequency, the wave-normal direction is nearly vertical and the ray direction is nearly horizontal.

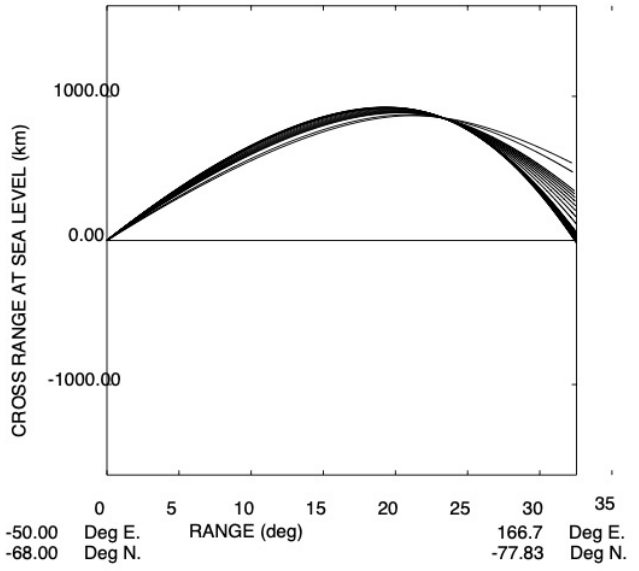

Figure 11: Projection of the ray paths from figure 10 on the ground. The great circle through the source and McMurdo Station is shown. The longitude and latitude of the two ends of the great-circle path are shown. The wave-normal direction of the wave that was transmitted at an elevation angle of −89.288° is 11.3° clockwise from north as it passes above McMurdo Station. This is reasonable agreement with the azimuth angle of 11° clockwise of north given by Chen et al. (2013).

Figure 12: Projection of the reverse ray paths on the ground. The height of the gravity wave over McMurdo is 98.935 km.

Reversing the wind direction for reverse ray tracing gives the ray paths in figure 15. Comparing with figure 12 shows the effect of changing the wind model.

The gravity waves measured at McMurdo showed gravity waves ranging from roughly 80 to 100 km in height. To compare with gravity waves measured at the lower height, we calculated the ray paths shown in figure 16.

6. Including spatially varying temperature and wind profiles

The next step is to include spatially varying temperature and wind profiles.

7. Conclusions

We made ray-path calculations and wavelength profile calculations for the 7.7-hour gravity wave that was observed at McMurdo, Antarctica on 29 June 2011.

The raypath calculations show some disagreement with the horizontal and vertical wavelengths measured at McMurdo on 29 June 2011 because the actual atmospheric conditions between the source and McMurdo must have differed from the conditions directly above McMurdo that we used to for the calculations. Differences in group velocities are attributed to the same cause.

However, there are qualitative results of the raypath calculations that give additional information about the source location. Because of the wind, the gravity waves do not follow a great circle path, but are bent considerably. Because of that, the actual source is probably not on the prime meridian, as was estimated by Chen et al. (2013), but more likely about 100° west of the

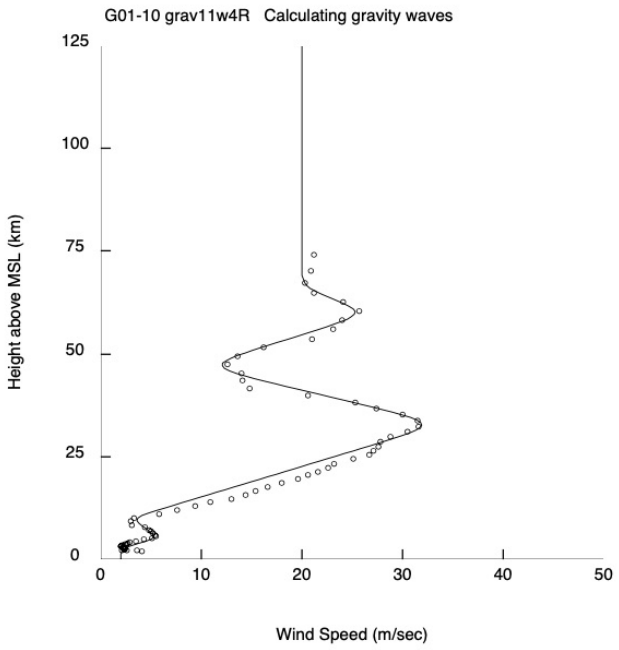

Figure 13: Wind speed profile used for the ray-path and profile calculations (solid line). Measured wind profile for 29 June 2011 from MERRA-2 (circles). The wind is blowing mostly toward the East.

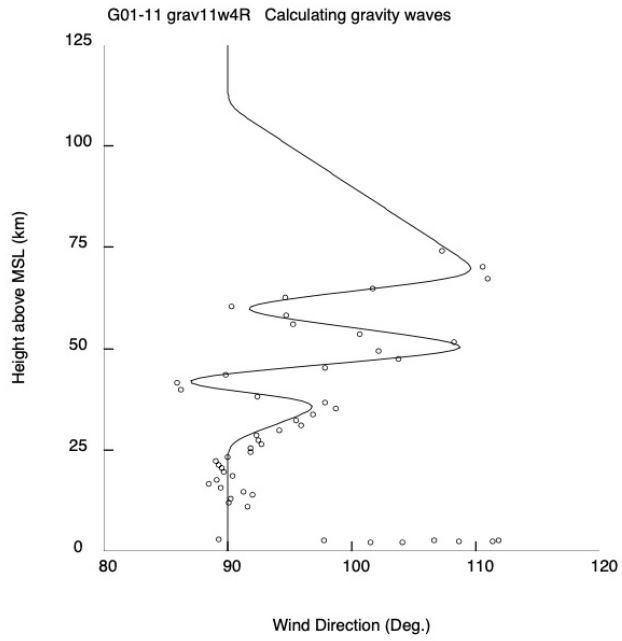

Figure 14: Wind direction profile used for the ray-path and profile calculations (solid line). Measured wind profile for 29 June 2011 from MERRA-2 (circles). This shows the direction (clockwise from North) that the wind is blowing toward.

Figure 15: Projection of the reverse ray paths on the ground using the wind model in figures 13 and 14. The height of the gravity wave over McMurdo is 98.935 km.

Figure 16: Projection of the reverse ray paths on the ground using the wind model in figures 13 and 14. The height of the gravity wave at McMurdo is 80 km. The elevation angle of the gravity wave over McMurdo varies from 89.430° (upper) to 89.434° (lower).

prime meridian. Because these gravity waves take several hours to propagate from the source to McMurdo, it might be necessary to take into account the time-variation in the atmospheric conditions as the wave propagates.

Calculation of the vertical wavelength profile, both for the conditions of the raypath calculations and for the conditions approximating the measured 7.7-hour gravity wave measured at McMurdo on 29 June 2011 show consistency between the calculations and the measurements.

Acknowledgments

This research was partially supported by the National Science Foundation (NSF) grants PLR-1246405 and AGS-1136272.

Appendix A. The usual dispersion relation ignores horizontal components of the Earth's angular velocity

The usual barotropic approximation to the acoustic-gravity wave dispersion relation is (Eckart, 1960, eq. (51-2), p. 125) (Gossard and Hooke, 1975, eq. (23-7), p. 112) (Jones, 2006, equation (1)):

$$(k_x^2 + k_y^2)(N^2 - \omega^2) - (\omega^2 - 4\Omega_z^2)(k_z^2 + \mathbf{k}_A^2 - \frac{\omega^2}{C^2}) = 0 \ , \quad \text{(A.1)}$$

where N is the Brunt-Väisälä frequency, $\omega = \sigma - \mathbf{k}\cdot\mathbf{U}$ is the intrinsic frequency, σ is the wave frequency, $\mathbf{U}$ is the background fluid velocity, $\mathbf{k}$ is the wavenumber, k_z is its vertical component, k_x and k_y are its horizontal components, Ω_z is the vertical component of the Earth's angular velocity, C is sound speed, and $\mathbf{k}_A \equiv \nabla\rho/(2\rho)$, where ρ is density.

Because the main Coriolis effect on the propagation of gravity waves is to give a low-frequency cutoff, and because that cutoff is correctly given by an approximation that neglects the effects of the horizontal components of the Earth's angular velocity, it made sense to use the simpler formula (A.1) based on that approximation before the wide-spread use of computers to make calculations. However, when making calculations with a computer, there is less advantage of a simple formula if a more accurate formula can give better results.

Appendix B. Including all components of the Earth's angular velocity in the Coriolis effect for the dispersion relation

Eckart (1960, sections 37-38, pp. 94-101) considers the horizontal components of the Earth's angular velocity and gives the appropriate equations, but does not calculate a dispersion relation that includes the horizontal components. Gossard and Hooke (1975, section 10, p. 50) also consider the possibility of including the horizontal components of the Earth's angular velocity in the Coriolis effect on the dispersion relation, but decide that the effect would be small. Jones (2006, equation (5)) gives a general formula for the acoustic-gravity-wave dispersion relation, including baroclinicity, rate-of-strain, and the Coriolis force (including all components of the Earth's angular velocity).

Equation (E.7), which gives an approximate dispersion relation that neglects rate-of-strain and baroclinicity, but still includes the effects of all components of the Earth's angular velocity on the Coriolis force, can be written

$$(\mathbf{k}^2 + \mathbf{k}_A^2)(N^2 - \omega^2) - \left(k_z^2 + k_A^2\right)N^2 + 4(\mathbf{k}_A\cdot\tilde{\mathbf{\Omega}})^2$$
$$+4(\mathbf{k}\cdot\tilde{\mathbf{\Omega}})^2 + 4\omega\tilde{\mathbf{\Omega}}\times\mathbf{\Gamma}\cdot\mathbf{k} + 1/C^2(\omega^4 - 4\omega^2\tilde{\mathbf{\Omega}}^2) = 0 \ , \quad \text{(B.1)}$$

where $\tilde{\mathbf{\Omega}} = \mathbf{\Omega} + \zeta/4$, $\zeta = \nabla\times\mathbf{U}$ is vorticity, and $\mathbf{\Omega}$ is the Earth's angular velocity.

Although the main Coriolis term (the first Coriolis term) in (B.1) agrees with the corresponding term in (A.1), other Coriolis terms in (B.1) differ because they depend on the horizontal components of the Earth's angular velocity.

Appendix C. Comparison

To compare ray paths calculated using the usual approximation (A.1) with the dispersion relation that includes Coriolis effects from all components of the Earth's angular velocity (B.1), we use a temperature profile appropriate to McMurdo, Antarctica for 29 June 2011, 20 UT, as shown in figure 1. The corresponding Brunt-Väisälä frequency profile is shown in figure 2.

Figure C.17 shows the ray paths in the North-South plane neglecting horizontal components of the Earth's angular velocity using the usual dispersion relation (A.1). Figure C.18 shows the corresponding ray paths using the dispersion relation that includes Coriolis effects from all components of the Earth's angular velocity (B.1). As can be seen, the rays are turned back at the same latitude in both figures C.17 and C.18, indicating that the low-frequency cut off for gravity waves depends only on the vertical component of the Earth's angular velocity. However, the ray paths in the two figures differ significantly, indicating that accurate calculation of ray paths requires including all components of the Earth's angular velocity in the dispersion relation.

In addition to comparing ray paths for the two versions of the dispersion relation, we can also compare profiles of vertical wavenumber and vertical wavelength. Figures C.19 and C.20 show a comparison of vertical-wavenumber profiles for the two versions of the dispersion relation. That they differ significantly is clear. Figures C.21 and C.22 show a comparison of vertical-wavelength profiles for the two versions of the dispersion relation. That they differ significantly is also clear. Figures C.23 and C.24 show a comparison of vertical-wavelength profiles for the two versions of the dispersion relation for a different elevation angle at the ground.

Because of horizontal gradients caused by the latitude-dependence of the Coriolis terms, there is not a one-to-one correspondence between the raypaths in figures C.17 and C.18 with the profiles in figures C.19 through C.24. However, both ray-path plots and profiles show that the turning-point height increases with elevation angle and that the turning-point heights for the dispersion relation that includes all components of the

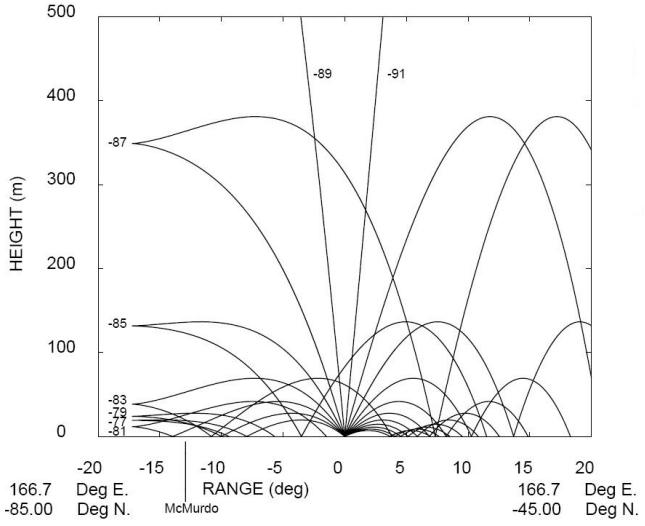

Figure C.17: Ray paths in the North-South plane neglecting horizontal components of the Earth's angular velocity for the Coriolis force in the dispersion relation. The source is on the ocean surface at a latitude of 65° South and a longitude of 166.67° East. The frequency is 23 μHz. The elevation angles of transmission (wave-normal direction) of the various rays are indicated in the figure, and are relative to propagation to the South. Negative elevation angles for the wave-normal direction correspond to upward ray propagation for gravity waves. McMurdo (as indicated in the figure) is located 12.83° South of the source.

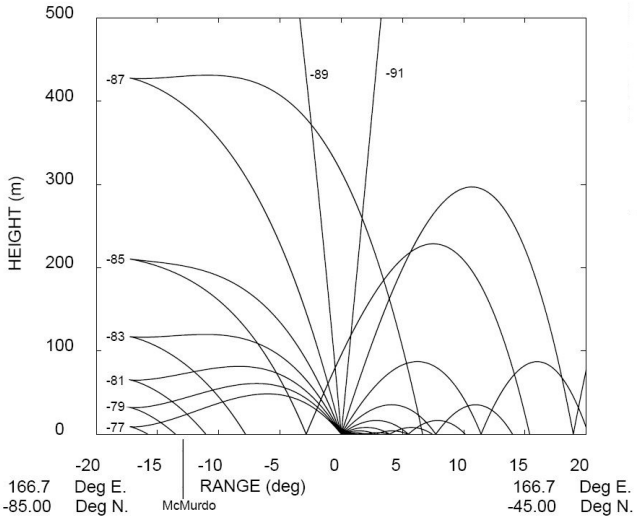

Figure C.18: Ray paths in the North-South plane including all components of the Earth's angular velocity for the Coriolis force in the dispersion relation. Otherwise, conditions are as in figure C.17.

Earth's angular velocity are higher than those when the effect of the horizontal components of the Earth's angular velocity are neglected.

Although the examples presented here do not include wind, the results are similar when wind is included.

Appendix D. Recommendation: include all components of the Earth's angular velocity when calculating Coriolis effects

Because there can be significant differences in both ray paths and vertical-wavelength profiles between dispersion relations that include or neglect the horizontal components of the Earth's angular velocity in the Coriolis terms, it is advisable to include all components of the Earth's angular velocity when calculating Coriolis effects on gravity-wave propagation.

Appendix E. Dispersion relation including all components of the Earth's angular velocity

Jones (2006, equation (5)) gives a general formula for the acoustic-gravity wave dispersion relation, including baroclinicity, rate-of-strain, and all components of the Earth's angular velocity on the Coriolis force. However, we start with (Jones, 2006, equation (10)), which neglects rate of strain in the dispersion relation as a special case of the general dispersion relation.

$$(\mathbf{k}^2 + \mathbf{k}_A^2)(N^2 - \omega^2) + \mathbf{k}\cdot\mathbf{S}\cdot\mathbf{k} + \mathbf{k}_A\cdot\mathbf{S}\cdot\mathbf{k}_A + \mathbf{A}\cdot\mathbf{k} + 1/C^2(\omega^4 - 4\omega^2\tilde{\mathbf{\Omega}}^2 + B^2/2 - 2i\omega\tilde{\mathbf{\Omega}}\cdot\mathbf{B}) = 0\,, \quad \text{(E.1)}$$

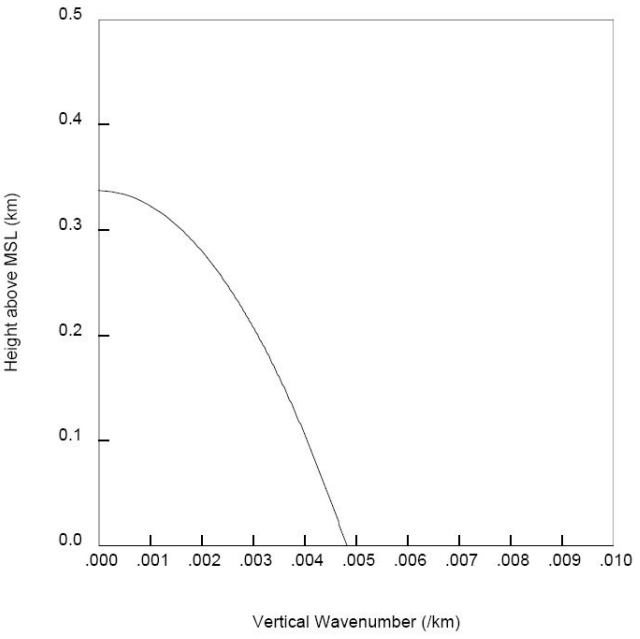

Figure C.19: Vertical-wavenumber profile at McMurdo (77.83° S, 166.67° E) neglecting horizontal components of the Earth's angular velocity for the Coriolis force in the dispersion relation. The frequency is 23 μHz. Propagation is toward the South. The elevation angle at the ground is −88.7°. The wave is evanescent above the turning point, the height where the wavenumber is equal to zero.

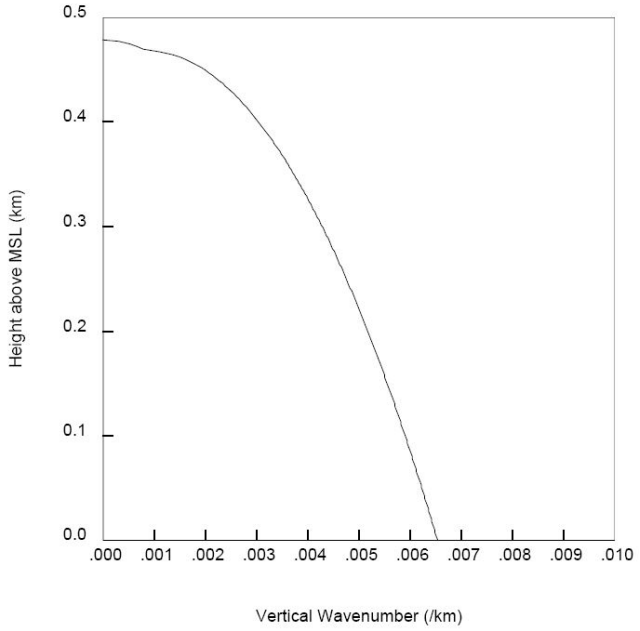

Figure C.20: Vertical-wavenumber profile at McMurdo including all components of the Earth's angular velocity for the Coriolis force in the dispersion relation. The elevation angle at the ground is −88.7°. Otherwise, conditions are as in figure C.19.

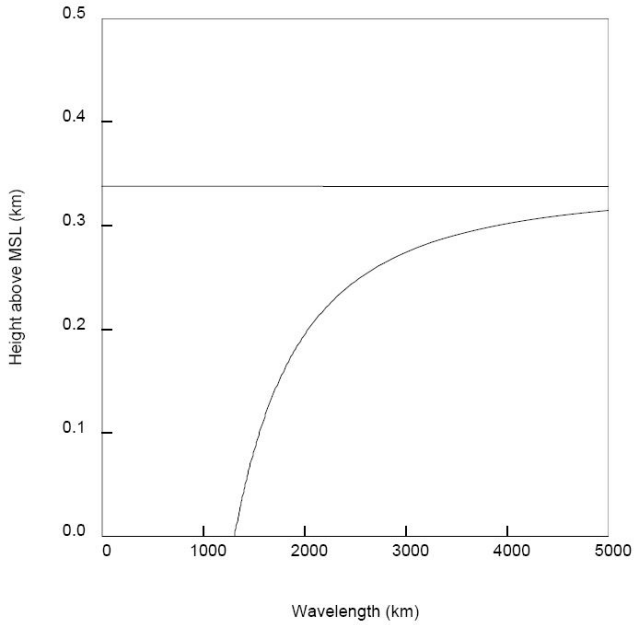

Figure C.21: Vertical-wavelength profile at McMurdo neglecting horizontal components of the Earth's angular velocity for the Coriolis force in the dispersion relation. The elevation angle at the ground is −88.7°. Otherwise, conditions are as in figure C.19. Because the vertical wavelength is proportional to the inverse of the vertical wavenumber, the vertical wavelength diverges at the turning point, as can be seen.

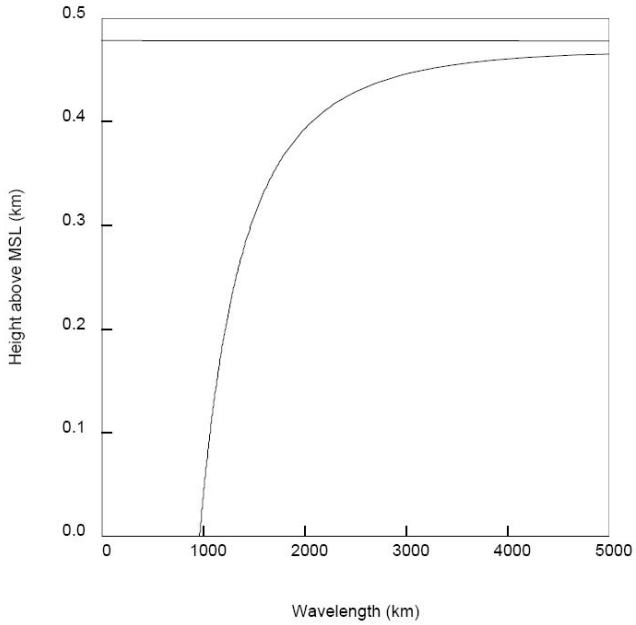

Figure C.22: Vertical-wavelength profile at McMurdo including all components of the Earth's angular velocity for the Coriolis force in the dispersion relation. The elevation angle at the ground is −88.7°. Otherwise, conditions are as in figure C.19.

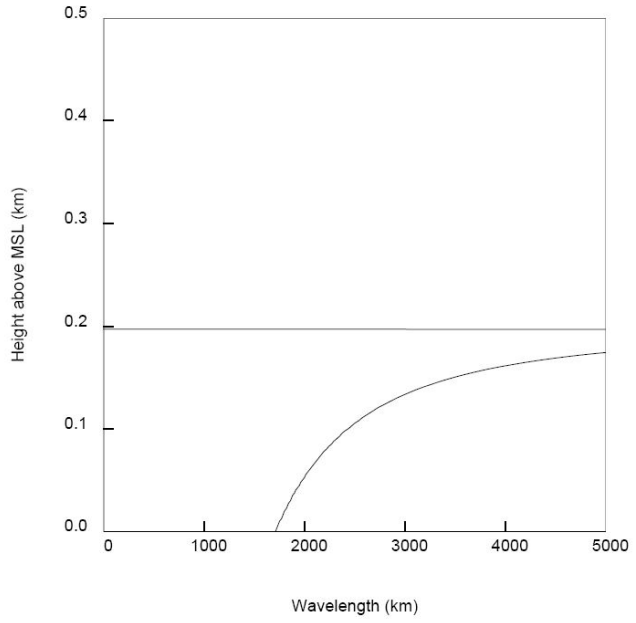

Figure C.23: Vertical-wavelength profile at McMurdo neglecting horizontal components of the Earth's angular velocity for the Coriolis force in the dispersion relation. The elevation angle at the ground is −88.3°. Otherwise, conditions are as in figure C.19.

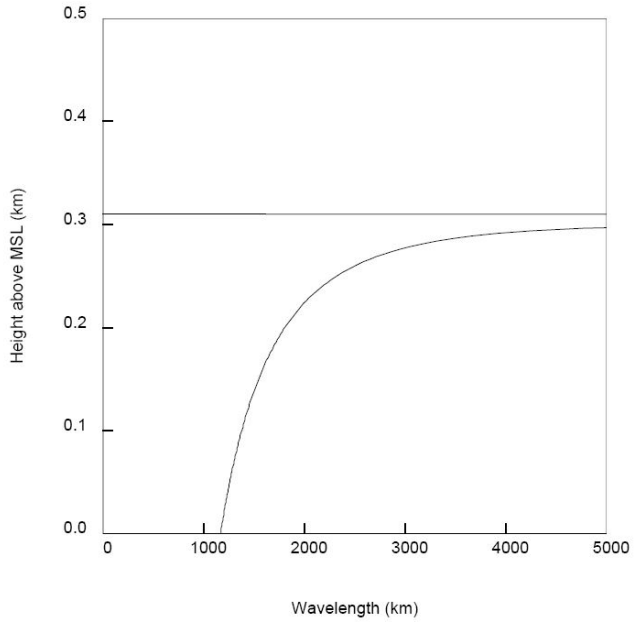

Figure C.24: Vertical-wavelength profile at McMurdo including all components of the Earth's angular velocity for the Coriolis force in the dispersion relation. The elevation angle at the ground is −88.3°. Otherwise, conditions are as in figure C.19.

where N is the Brunt-Väisälä frequency[2], $\mathbf{g}$ is the acceleration due to gravity, $\omega = \sigma - \mathbf{k}\cdot\mathbf{U}$ is the intrinsic frequency, σ is the wave frequency, $\mathbf{U}$ is the background fluid velocity, $\mathbf{k}$ is the wavenumber, $\mathbf{B}$ is the baroclinic vector, $\tilde{\mathbf{\Omega}} = \mathbf{\Omega} + \zeta/4$, where $\zeta = \nabla\times\mathbf{U}$ is vorticity, $\mathbf{\Omega}$ is the Earth's angular velocity, C is sound speed, $\mathbf{k}_A \equiv \nabla\rho/(2\rho)$, where ρ is density, $\mathbf{S}$ is the symmetric matrix defined by

$$S_{\alpha\beta} = \underbrace{-\frac{1}{2\rho}\left(\frac{\partial\tilde{\rho}_{pot}}{\partial x_\alpha}\tilde{g}_\beta + \frac{\partial\tilde{\rho}_{pot}}{\partial x_\beta}\tilde{g}_\alpha\right)}_{1} \underbrace{+4\tilde{\Omega}_\alpha\tilde{\Omega}_\beta}_{2} + \underbrace{\frac{i}{\omega}\left(\tilde{\Omega}_\alpha B_\beta + \tilde{\Omega}_\beta B_\alpha\right)}_{3} , \tag{E.2}$$

$\tilde{\mathbf{g}} \equiv \nabla p/\rho = \mathbf{g} - D\mathbf{U}/Dt - 2\mathbf{\Omega}\times\mathbf{U}$ is the effective vector acceleration due to gravity [including (minus) the acceleration of the background flow], $\tilde{\rho}_{pot}$ is local potential density, defined by $\nabla\tilde{\rho}_{pot} = \nabla\rho - \nabla p/C^2$ (Jones, 2005, 2008a), p is pressure,

$$\mathbf{A} = (4\omega\tilde{\mathbf{\Omega}} + i\mathbf{B})\times\mathbf{\Gamma} + 2\mathbf{k}_A\cdot\tilde{\mathbf{\Omega}}\mathbf{B}/\omega , \tag{E.3}$$

and $\mathbf{\Gamma} = \mathbf{k}_A - \tilde{\mathbf{g}}/C^2$ is the vector generalization Jones (2001, 2012) of Eckart's coefficient (Gossard and Hooke, 1975, p. 90).

Term 2 in (E.2) is a Coriolis term, which we will be keeping. Term 3 in (E.2) is a baroclinic and Coriolis term, which we shall be neglecting when we neglect baroclinic terms.

[2]The Brunt-Väisälä frequency, N, is calculated from $N^2 = \nabla\tilde{\rho}_{\rm pot}\cdot\tilde{\mathbf{g}}/\rho = (\nabla\rho - \nabla p/C^2)\cdot\tilde{\mathbf{g}}/\rho$, where $\tilde{\rho}_{\rm pot}$ is local potential density, p is pressure, C is sound speed, $\tilde{\mathbf{g}} = \nabla p/\rho$ is the effective acceleration due to gravity

Neglecting the baroclinic terms in (E.1), (E.2), and (E.3) gives

$$(\mathbf{k}^2 + \mathbf{k}_A^2)(N^2 - \omega^2) + \mathbf{k}\cdot\mathbf{S}\cdot\mathbf{k} + \mathbf{k}_A\cdot\mathbf{S}\cdot\mathbf{k}_A + \mathbf{A}\cdot\mathbf{k} + 1/C^2(\omega^4 - 4\omega^2\tilde{\mathbf{\Omega}}^2) = 0 , \tag{E.4}$$

where $\mathbf{S}$ is the symmetric matrix defined by

$$S_{\alpha\beta} = \underbrace{-\frac{1}{2\rho}\left(\frac{\partial\tilde{\rho}_{pot}}{\partial x_\alpha}\tilde{g}_\beta + \frac{\partial\tilde{\rho}_{pot}}{\partial x_\beta}\tilde{g}_\alpha\right)}_{1} \underbrace{+4\tilde{\Omega}_\alpha\tilde{\Omega}_\beta}_{2} , \tag{E.5}$$

and

$$\mathbf{A} = 4\omega\tilde{\mathbf{\Omega}}\times\mathbf{\Gamma} . \tag{E.6}$$

Substituting (E.5) and (E.6) into (E.4) gives

$$(\mathbf{k}^2 + \mathbf{k}_A^2)(N^2 - \omega^2) - \tfrac{1}{\rho}\mathbf{k}\cdot\nabla\tilde{\rho}_{pot}\,\tilde{\mathbf{g}}\cdot\mathbf{k} - \tfrac{1}{\rho}\mathbf{k}_A\cdot\nabla\tilde{\rho}_{pot}\,\tilde{\mathbf{g}}\cdot\mathbf{k}_A + 4(\mathbf{k}\cdot\tilde{\mathbf{\Omega}})^2 + 4(\mathbf{k}_A\cdot\tilde{\mathbf{\Omega}})^2 + 4\omega\tilde{\mathbf{\Omega}}\times\mathbf{\Gamma}\cdot\mathbf{k} + 1/C^2(\omega^4 - 4\omega^2\tilde{\mathbf{\Omega}}^2) = 0 \tag{E.7}$$

for the acoustic-gravity-wave dispersion relation in which all components of the Earth's angular velocity are included in the Coriolis terms.

References

Bedard, Jr., A. J., Jones, R. M., 2013. Infrasonic ray tracing applied to mesoscale atmospheric structures: Refraction by hurricanes. J. Acoust. Soc. Am. 134 (5), 3446–3451.

Brillouin, L., 1926. La mécanique ondulatoire de Schrödinger; une méthode générale de résolution par approximations successives. Academie des sciences, Paris 183, 24–26.

Chen, C., Chu, X., McDonald, A. J., Vadas, S. L., Yu, Z., Fong, W., Lu, X., 2013. Inertia-gravity waves in antarctica: A case study using simultaneous lidar and radar measurements at McMurdo/Scott Base (77.8°S, 166.7°E). Journal of Geophysical Research: Atmospheres 118 (7), 2794–2808.
URL http://dx.doi.org/10.1002/jgrd.50318

Chen, C., Chu, X., Zhao, J., Roberts, B. R., Yu, Z., Fong, W., Lu, X., Smith, J. A., 2016. Lidar observations of persistent gravity waves with periods of 3-10 h in the Antarctic middle and upper atmosphere at McMurdo (77.83°S, 166.67°E). Journal of Geophysical Research: Space Physics 121 (2), 1483–1502, 2015JA022127.
URL http://dx.doi.org/10.1002/2015JA022127

Chu, X., Yu, Z., Gardner, C. S., Chen, C., Fong, W., 2011. Lidar observations of neutral Fe layers and fast gravity waves in the thermosphere (110-155 km) at McMurdo (77.8°S, 166.7°E), antarctica. Geophysical Research Letters 38 (23), L23807.
URL http://dx.doi.org/10.1029/2011GL050016

Chu, X., Zhao, J., Lu, X., Harvey, V. L., Jones, R. M., Chen, C., Fong, W., Yu, Z., Roberts, B. R., Dörnbrack, A., 2018. Lidar observations of stratospheric gravity waves from 2011 to 2015 at McMurdo (77.84°S, 166.69°E), Antarctica: 2. Potential energy densities, lognormal distributions, and seasonal variations. Journal of Geophysical Research: Atmospheres 123 (15), 7910–7934.

Eckart, C., 1960. Hydrodynamics of Oceans and Atmospheres. Pergamon Press, Oxford.

Georges, T. M., Jones, R. M., Lawrence, R. S., 1990. A PC version of the HARPO ocean acoustic ray-tracing program. Tech. Memo ERL WPL-180, Natl. Oceanic and Atmos. Admin., Boulder, Colorado, 18 pp. (program available at http://cires.colorado.edu/~mjones/raytracing/programs.htm).

Gossard, E. E., Hooke, W. H., 1975. Waves in the Atmosphere. Elsevier Scientific Publishing Company, Amsterdam.

Hickey, M., Cole, K., 1987. A quartic dispersion equation for internal gravity waves in the thermosphere. Journal of Atmospheric and Terrestrial Physics 49 (9), 889 – 899, http://dx.doi.org/10.1016/0021-9169(87)90003-1.

Jeffreys, H., 1923. On certain approximate solutions of linear differential equations of the second order. Proc. London, Math. Soc. Ser. 2 23, 428–436.

Jones, R. M., 1996. Three dimensional ray tracing in the atmosphere. In: W. Dieminger, G. Hartmann, R. Leitinger (Eds.), THE UPPER ATMOSPHERE. Springer Verlag, Berlin-Heidelberg, Ch. II.3.1.4, pp. 307–327, errata available at (Jones, 2007, `http://cires.colorado.edu/~mjones/pubs/errata2.htm`, date last viewed 4 April 2018).

Jones, R. M., 2001. The dispersion relation for internal acoustic-gravity waves in a baroclinic fluid. Physics of Fluids 13, 1274–1280, errata available at (Jones, 2012, `http://cires.colorado.edu/~mjones/pubs/errata9.pdf`, date last viewed 4 April 2018).

Jones, R. M., November 2005. A general dispersion relation for internal gravity waves in the atmosphere or ocean, including baroclinicity, vorticity, and rate of strain. J. Geophys. Res. 110, D22106, doi: 10.1029/2004JD005654, Errata available at (Jones, 2008a, `http://cires.colorado.edu/~mjones/pubs/errata7.pdf`, date last viewed 4 April 2018).

Jones, R. M., November 2006. Minimum and maximum propagation frequencies for internal gravity waves. J. Geophys. Res. 111, D06109, doi: 10.1029/2005JD006189, Errata available at (Jones, 2008b, `http://cires.colorado.edu/~mjones/pubs/errata8.pdf`, date last viewed 4 April 2018).

Jones, R. M., 2007. Errata: Three dimensional ray tracing in the atmosphere, pp. 307-327 in THE UPPER ATMOSPHERE, editors W. Dieminger, G. Hartmann, and R. Leitinger, springer verlag, berlin-heidelberg 1996, 1014 pages., errata available at `http://cires.colorado.edu/~mjones/pubs/errata2.htm` (date last viewed 4 April 2018).

Jones, R. M., 2008a. Errata: A general dispersion relation for internal gravity waves in the atmosphere or ocean, including baroclinicity, vorticity, and rate of strain, *J. Geophys. Res.*, 2005, doi: 10.1029/2004JD005654, Errata available at `http://cires.colorado.edu/~mjones/pubs/errata7.pdf` (date last viewed 4 April 2018).

Jones, R. M., 2008b. Errata: Minimum and maximum propagation frequencies for internal gravity waves, *J. Geophys. Res.*, 2006, doi: 10.1029/2005JD006189, Errata available at `http://cires.colorado.edu/~mjones/pubs/errata8.pdf` (date last viewed 4 April 2018).

Jones, R. M., 2012. Errata: The dispersion relation for internal acoustic-gravity waves in a baroclinic fluid, *Physics of Fluids*, 2001, 1274-1280, Errata available at `http://cires.colorado.edu/~mjones/pubs/errata9.pdf` (date last viewed 4 April 2018).

Jones, R. M., Bedard, Jr., A. J., 2015. Infrasonic ray tracing applied to small-scale atmospheric structures: Thermal plumes and updrafts/downdrafts. J. Acoust. Soc. Am. 137 (2), 625–632.

Jones, R. M., Bedard, Jr., A. J., 2018. Atmospheric gravity wave ray tracing: Ordinary and extraordinary waves. Journal of Atmospheric and Solar-Terrestrial Physics 179, 342 – 357.

Jones, R. M., Riley, J. P., Georges, T. M., 1986a. HARPA - A versatile three-dimensional Hamiltonian ray-tracing program for acoustic waves in the atmosphere above irregular terrain. NOAA Special Report, GovDoc No. C55.602:H 18; GPO Item No. 207-C-1; PB87132031, National Oceanic and Atmospheric Administration, Boulder, Colorado, 410 pp., report available at `http://cires.colorado.edu/~mjones/pubs/harpa.pdf` (date last viewed 4 April 2018), program available at `http://cires.colorado.edu/~mjones/raytracing` (date last viewed 4 April 2018).

Jones, R. M., Riley, J. P., Georges, T. M., 1986b. HARPO - A versatile three-dimensional Hamiltonian ray-tracing program for acoustic waves in an ocean with irregular bottom. NOAA Special Report, GovDoc No. C55.602:H 23; GPO Item No. 0207-C-01; PB87172573, National Oceanic and Atmospheric Administration, Boulder, Colorado, 455 pp., report available at `http://cires.colorado.edu/~mjones/pubs/harpo.pdf` (date last viewed 4 April 2018), program available at `http://cires.colorado.edu/~mjones/raytracing` (date last viewed 4 April 2018).

Kramers, H. A., 1926. Wellenmechanik und halbzahlige Quantisierung. Z. Phys. 39, 828–840.

Liouville, J., 1836. Sur le développement des fonctions ou parties de fonctions en séries dont les divers termes sont assujettis à satisfaire à une même équation différentielle du second ordre contenant un paramètre variable, I. J. Math. Pur Appl. 1, 253–265.

Liouville, J., 1837a. Sur le développement des fonctions ou parties de fonctions en séries dont les divers termes sont assujettis à satisfaire à une même équation différentielle du second ordre contenant un paramètre variable, II. J. Math. Pur Appl. 2, 16–35.

Liouville, J., 1837b. Sur le développement des fonctions ou parties de fonctions en séries dont les divers termes sont assujettis à satisfaire à une même équation différentielle du second ordre contenant un paramètre variable, III. J. Math. Pur Appl. 2, 418–436.

NRLMSISE-00, Community Coordinated Modeling Center, 2016. NRLMSISE-00 Atmosphere Model, http://ccmc.gsfc.nasa.gov/modelweb/models/nrlmsise00.php.

Phillips, N. A., 1966. The equations of motion for a shallow rotating atmosphere and the "traditional approximation". Journal of the Atmospheric Sciences 23 (5), 626–628, doi:10.1175/1520-0469(1966)023<0626:TEOMFA>2.0.CO;2.

Rayleigh (John William Strutt), L., 1912. On the propagation of waves through a stratified medium, with special reference to the question of reflection. Proc. Royal Soc. A 86, 207–226.

Wentzel, G., 1926. Eine Verallgemeinerung der Quantenbedingungen für die Zwecke der Wellenmechanik. Z. Phys. 38, 518–529.

Zhao, J., Chu, X., Chen, C., Lu, X., Fong, W., Yu, Z., Jones, R. M., Roberts, B. R., Dörnbrack, A., 2017. Lidar observations of stratospheric gravity waves from 2011 to 2015 at McMurdo (77.84°S, 166.69°E), Antarctica: 1. Vertical wavelengths, periods, and frequency and vertical wave number spectra. Journal of Geophysical Research: Atmospheres 122 (10), 5041–5062, 2016JD026368.
URL `http://dx.doi.org/10.1002/2016JD026368`